Uncertainty budget for detector-based absolute radiometric calibration with GLAMR

ZHIPENG WANG,[1,*] JULIA BARSI,[2] KURTIS THOME,[2]
BRIAN N. WENNY,[1] BRENDAN MCANDREW,[2] BORYANA EFREMOVA,[3]
AND JOEL MCCORKEL[2]

[1] *Science Systems and Applications, Inc., Lanham, MD 20706*
[2] *NASA/GSFC/Sciences and Exploration Directorate, Greenbelt, MD 20771*
[3] *GeoThinkTank, LLC, Washington, DC 20009*
[*] *zhipeng.wang@nasa.gov*

Abstract: The accuracy of the absolute radiometric calibration (RadCal) for remote sensing instruments is essential to their wide range of applications. The uncertainty associated to the traditional source-based RadCal method is assessed at a 2% (k=1) or higher level for radiance measurement. To further improve the accuracy to meet the demands of climate studies, a detector-based approach using tunable lasers as a light source has been devised. The Goddard Laser for Absolute Measurement of Radiance, known as the GLAMR system, is a notable example of the incorporation of such technology. Using transfer radiometers calibrated at NIST as calibration standards, the absolute spectral response (ASR) function of a remote sensing instrument is measured with its uncertainty traceable to the International System of Units. This paper presents a comprehensive uncertainty analysis of the detector-based absolute RadCal using the GLAMR system. It identifies and examines uncertainty sources during the GLAMR RadCal test, including those from the GLAMR system, the testing configuration, and data processing methodologies. Analysis is carried out to quantify the contribution of each source and emphasize the most influential factors. It is shown that the calibration uncertainty of GLAMR RadCal can be better than 0.3% (k=1) in the wavelength range of 350-950 nm and 0.6% (k=1) between 950-2300 nm, with the exception of regions with strong water absorption. In addition, recommendations are made to refine the calibration process to further reduce the uncertainty.

1. Introduction

Radiometric calibration (RadCal) of remote sensing instrument is essential for the accurate conversion of detector response into spectral radiance, which directly affects the accuracy and reliability of the downstream products. Within the reflective solar spectrum of 350-2500 nm, most state-of-the-art instruments have been calibrated pre-launch via the source-based approach using a light source of known radiance as a benchmark for calibration. Table 1 summarizes the uncertainty (UC) levels of some of these instruments. Generally, their accuracy in radiance is estimated to be no better than 2% with a coverage factor k=1, largely bounded by the capability of the source-based approach [1]. The assessed uncertainty levels can be even higher for certain spectral bands affected by various artifacts.

The necessity for enhanced RadCal techniques that maintains the traceability to the International System of Units (SI), are becoming increasingly important due to the rapidly expanding use of satellite-borne remote sensing across a wide range of environmental applications. For example, to distinguish the long-term climate changes and the uncertainty of natural variations, an absolute uncertainty of 0.15% (k=1) in measurements of the reflected solar spectral region is deemed necessary [2]. The Climate Absolute Radiance and Refractivity Observatory (CLARREO) Pathfinder, or CPF, mission incorporates this finding in the design and manufacture of its principal instrument, the HyperSpectral Imager for Climate Science (HySICS) [3]. The radiometric accuracy requirement for HySICS, an Offner-Chrisp imaging spectrometer, is set at 0.3% (k=1) across its entire spectral range of 350-2300 nm [4]. Thus, there is a clear need for the

development and incorporation of an absolute RadCal strategy capable of achieving this level of accuracy, which is a significant advancement over the conventional approach.

Table 1. Overview of the radiometric calibration uncertainty (k=1) for reflective solar bands for representative satellite-borne remote sensing instruments

Instrument	Platform	Launch Year	UC Specified	UC Assessed
MODIS	Terra/Aqua	1999/2002	2% (R*) 5% (L)	1.6%-2.2% [5, 6]
VIIRS	S-NPP/NOAA-20/21	2011/2017/2022	2% (R)	1.2%-1.9% [7–11]
OLI	Landsat-8/9	2013/2021	3% (R) 5% (L)	2.5% [12, 13]
OLCI	Sentinel-3 A/B	2016/2018	2% (R)	1.4%-1.9% [14, 15]
HySICS	ISS	2025 (TBC)	0.3% (R)	N/A

*: R->reflectance; L->radiance

Tunable laser systems, known for their high power, low wavelength uncertainty, and narrow bandwidth, have been in use since the early 1980s as sources of radiant flux for calibrating a wide array of light-measuring instruments. At the National Institute of Standards and Technology (NIST), a tunable laser scanning system known as SIRCUS, or Spectral Irradiance and Radiance responsivity Calibrations using Uniform Sources, has been developed. It consists of tunable, computer-controlled lasers that covers a broad spectrum ranging from 210 nm to 2500 nm [16, 17]. The SIRCUS systems have been utilized to conduct the optical power responsivity comparison between the nation′s standard for optical power, the Primary Optical Watt Radiometer (POWR), and transfer standard detectors, and then to calibrate the instrument under test by measuring the absolute spectral responses (ASRs) of detectors with uniform light sources, typically generated by coupling the laser light into integrating spheres.

Another version of SIRCUS capable of traveling has been developed at National Aeronautics and Space Administration (NASA)′ Goddard Space Flight Center (GSFC) and named as , the Goddard Laser for Absolute Measurement of Radiance (GLAMR), GLAMR has a track record of successful calibration of multiple airborne and spaceborne remote sensing instruments, including the Visible Infrared Imaging Radiometer Suite (VIIRS) onboard the Joint Polar Satellite System (JPSS)-2, 3, and 4 , Operational Land Imager (OLI) onboard Landsat-8 , Operational Land Imager (OLI)-2 onboard Landsat-9 and the Ocean Color Instrument (OCI) for the Plankton, Aerosol, Cloud, ocean Ecosystem (PACE) mission [18–20]. However, in all these tasks, the primary assignment to the GLAMR calibration has been solely on the measurements of the relative spectral response (RSR) of the instrument. To date, the capability of the absolute RadCal with GLAMR to deliver low uncertainty calibration has only been tested in the calibration of the SOlar, Lunar Absolute Reflectance Imaging Spectroradiometer (SOLARIS), which had been a concept demonstration system for CLARREO mission [21].

Before its broader adoption as an absolute radiometric calibration methodology, understanding the uncertainty associated with the detector-based absolute RadCal process using the GLAMR system is crucial to determine the accuracy and dependability of the collected data. In this paper, this uncertainty is systematically assessed, taking into account the various components in the calibration process. The overall uncertainty budget of the GLAMR RadCal is developed and presented. The results can form a foundation for future advancements and refinements in the RadCal techniques, ensuring the highest possible accuracy in Earth observation data. Unless specified otherwise, the uncertainty values presented in this paper correspond to k=1. The structure of the paper is organized in the following manner: In Section 2, the method of detector-based calibration is outlined, along with its recent implementation at NASA GSFC

as the GLAMR system. Section 3 introduces the methods of data collection and processing implemented to the calibration. A detailed examination of the uncertainty sources associated with GLAMR RadCal is provided in Section 4. In Section 5, we propose the overall uncertainty budget and discuss potential enhancements of the calibration process to reduce its uncertainty. Finally, conclusions and recommendations for future work on the uncertainty analysis are given in Section 6.

2. Detector-based RadCal with GLAMR

2.1. Detector-based calibration approach

In the RadCal process for remote sensing instruments, calibration sources with known optical power levels are used to illuminate the device under test (DUT), that establishes a relationship between the instrument′ response and SI physical units of the calibration source. The calibration standards directly used in the RadCal can be seen as secondary transfer standards since they provide a transfer of the physical quantify of the primary standard, a reference device that is traceable to the fundamental SI units, to the calibration lab, and subsequently to the DUT [22–24]. The uncertainty of the calibration generally increases along this calibration chain. Depending on the types of calibration standards used, there are two common methods to perform RadCal in absolute scale: source-based and detector-based. The standard for the traditional source-based approach is an optical source being calibrated with traceability to the optical power. The source illuminates the DUT at pre-set radiance levels, and the relationship between the source′s output and the DUT′s output is then created to derive the calibration equations and related parameters. The fundamental assumption for the source-based approach is that the output of the source remains stable over time, specifically between its own calibration and the calibration of the DUT. On the other hand, the detector-based calibration leverages a light source, calibrated in the same calibration lab as the DUT using a calibration detector package whose traceability is created by an earlier calibration against the primary standard in a separate lab. The calibration of the DUT is achieved by comparing the outputs of the DUT detectors and the calibration detectors,

The foundation of the detector-based approach is that, when used under consistent measurement geometries even in different test sites, the detector package remain stable. This is generally true for semiconductor detectors known for their robustness and superior long-term stability, requiring less maintenance and are less likely to be affected by the transportation of calibration standards between labs. These qualities contrast with the optical radiation sources that demand extensive maintenance and careful handling, making them less practical in comparison. This stability ensures the calibration traceability to the SI can be reliably maintained between sites. Another major advantage of implementing the detector-based approach is that it enables the usage of tunable lasers as the optical source. Unlike conventional lamp calibration that uses a broadband source, the usage of a near-monochromatic source eliminates the need for a spectral filter, often the largest source of uncertainty to the RadCal, to disperse light along the optical path. In addition, the high output power of the laser sources can boost the signal-to-noise ratio (SNR) of the calibration. For the characterization of low-response systems, like those associated to high spectral or spatial resolutions, this elevation is particularly essential.

2.2. GLAMR system

The GLAMR team of calibration scientists at NASA GSFC developed the GLAMR system from a traveling version of SIRCUS (T-SIRCUS) and are responsible for maintaining and operating the system [25]. A sketch of the basic components of the GLAMR system is shown in Fig. 1. The GLAMR system comprises a suite of tunable laser sources, including several configurations of custom Optical Parametric Oscillators (OPOs) and two commercial lasers that span 340 to 2500 nm. The custom OPO lasers utilize a frequency doubled Nd:VO_4 laser operating at a wavelength

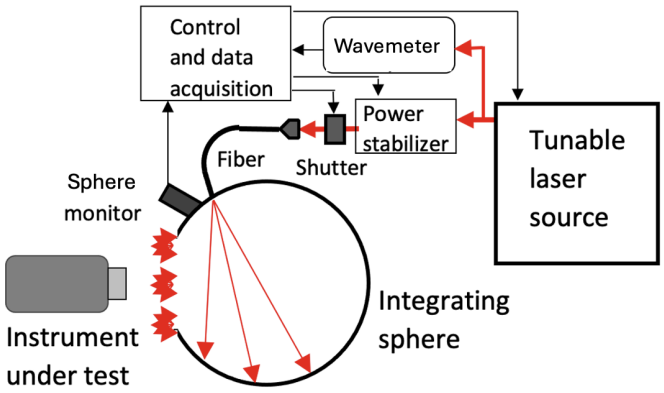

Fig. 1. Basic components of the GLAMR system.

of 532 nm as a pump source for two lithium triborate (LBO) based OPO's producing output energy across a range of tunable wavelengths. These systems are mode locked with a pulse repetition frequency of either 76 or 80 MHz, depending on which pump laser is being used. Temporal averaging of light in the integrating sphere overlaps these pulses into a continuous waveform with a 20% amplitude ripple at the mode locking frequency [26]. There are also two commercial systems with continuous wave operation. One is the ARGOS tunable OPO manufactured by Aculight Corporation. The other is the CLT series manufactured by IPG Photonics Corporation, a Cr:ZnSe/S laser. Together they provide complete redundancy for wavelengths above 2200 nm [19, 27]. Table 2 summarizes the spectral coverage of these laser types.

Four distinct optical benches, referred to as OPO Laser Alignment Facilities (OLAFs) 1-4, have been developed by the GLAMR team, each hosting a GLAMR laser system to ensure redundancy. Embedded on each bench are two separate configurations of OPOs for near-infrared (NIR) and short-wave infrared (SWIR) regions respectively, and they together cover the spectral range below 2200 nm. They use a common pump laser and identical OPO crystals but have slightly different tuning ranges due to unique mirror coatings. Multiple wavelength ranges are available from each OPO using the resonant wavelength, non-resonant idler wavelength, or second harmonic generation (SHG) of the resonant wavelength, which are the laser configurations referenced in Table 2.

Table 2. The wavelength ranges covered by various GLAMR lasers [20]

Laser Configuration	Configuration ID	Wavelength Range (nm)
OPO Second Harmonic (LBO for NIR)	OPO_NIR_SHG	340-550
OPO Second Harmonic (LBO for SWIR)	OPO_SWIR_SHG	550-700
OPO Fundamental (LBO for NIR)	OPO_NIR	700-1100
OPO Fundamental (LBO for SWIR)	OPO_SWIR	1100-1200
OPO Idler (LBO for NIR)	OPO_NIR_Idler	1200-2200
Commercial OPO	CLT	1900-2500
Commercial Cr:ZnSe/S	ARGOS	2185-2500

Within the system, the laser beam is directed through an intensity stabilizer that controls the relative optical power in the beam to better than 0.1% of the set point. A portion of the laser beam is sent to a wavemeter, specifically a Bristol spectrum analyzer, which measures the center wavelength and linewidth of the radiation to within 0.02 nm. Full spectra are also recorded when using the several laser configurations to measure the bandwidth and mode stability. Spectral monitoring of the CLT is used to check the amplitude of the spectral side lobes, which are produced within approximately ±3 nm of the dominant wavelength and contain as much as a few percent of the total power. A measurement must be re-done if the laser output is unstable or the side lobe in its spectrum is excessively strong. A mechanical shutter is placed in the beam path before the light is coupled to an optical fiber, allowing the swift acquisition of the instrument detector′ responses with or without laser light with the shutter open or closed. Most control of the lasers and the shutter is done via a software interface, which can also be synchronized with operation of the DUT if desired. A multi-mode optical fiber is used to deliver the radiant flux from the laser table to a 30-inch Polytetrafluoroethylene (PTFE) integrating sphere to illuminate the DUT′s entrance pupil uniformly. Through tuning the lasers across the spectral range of the DUT, a full evaluation of spatial and spectral characteristics of the DUT is accomplished.

The radiance within the sphere is monitored by three radiometers of different types: silicon, InGaAs, and extended InGaAs, which collectively covers the entire spectral range of GLAMR system. A feedback signal from the radiometer is sent to the laser power stabilizer, as shown in Fig. 1, to maintain constant radiance in the integrating sphere. One advantage of using feedback from the sphere itself to stabilize radiance is that any fluctuation due to mechanical vibration at the fiber coupling can be suppressed. A second advantage is compensation for sphere loading, a condition where light scattered from the DUT is directed back into the sphere. Work with the SMs in collaboration with NIST has shown that the SMs are both stable and can be calibrated with low absolute uncertainties. These radiometers are internally designated as sphere monitors (SM) to be distinguished from the transfer radiometers (TRs) that are utilized as the calibration standard, which are another set of three radiometers along with accessory components consisting of a temperature controller and an amplifier. The TRs are manufactured by L-1 Standards and Technology, Inc., and also use silicon for the 340 to 950 nm range, InGaAs for the 950 to 1600 nm range, and extended InGaAs for the 1600 to 2500 nm range, respectively. Both SMs and TRs are temperature stabilized and use photodiodes in photovoltaic mode as their photosensitive elements.

2.3. GLAMR RadCal configuration

The GLAMR RadCal is typically only one component of a comprehensive RadCal for a remote sensing instrument. The GLAMR system is designed with the capability of being transported to the testing site of the instrument. This eliminates the necessity of relocating the DUT, and thus mitigates any risks associated with transportation of the DUT and ground system and preserves the DUT's test conditions. The basic configuration of the GLAMR RadCal is shown in Fig. 2.

The detector-based RadCal process involves two stages to establish SI-traceability and ensure the calibration accuracy:

1. Prior to the calibration of the DUT, a sphere calibration is run to transfer the NIST-traceable radiometric scale to the SMs. In the process of sphere calibration, the TRs are precisely positioned to face the exit port of the GLAMR integrating sphere, using custom built alignment guides to ensure repeatability of alignment across multiple sphere calibrations. The sphere calibration should be performed with all the optical elements to be used in the instrument test, when possible. For example, in the case of an instrument to be calibrated under vacuum conditions, the vacuum chamber window should be included between the sphere and transfer radiometers.
2. At the stage of DUT calibration, the GLAMR sphere is situated in front of the DUT to illuminate the instrument. The sphere is aligned to the DUT′s optical axis to ensure full field and

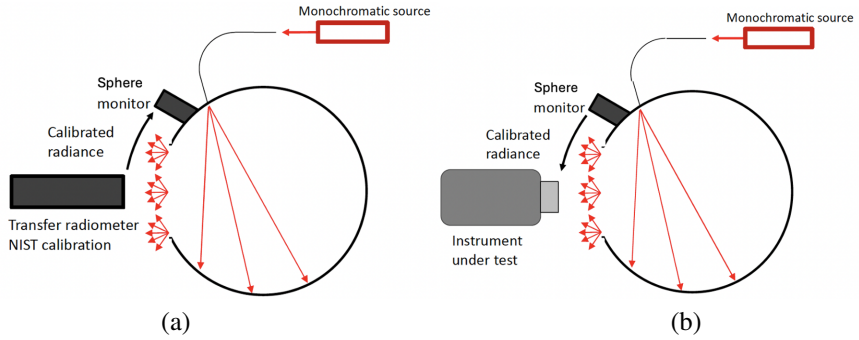

Fig. 2. The basic configuration of the GLAMR system during RadCal for (a) sphere calibration; (b) instrument calibration.

full aperture illumination. Also the illumination geometry for the DUT is matched to that for the TR during the sphere calibration. GLAMR can support a test with the instrument in a thermal vacuum chamber, in a clean room or uncontrolled conditions.
Provided the calibration schedule permits, it is advantageous to run an additional sphere calibration following the DUT calibration to verify the stability of the GLAMR system throughout the testing period.

During both stages, the GLAMR source is tuned in small, pre-set wavelength steps. This wavelength tuning is accomplished by software control of the crystal temperatures and optical path through dispersion prisms, following tuning parameter look-up tables that are manually generated. The wavelength step size is determined by the instrument requirements. For recent tests, step sizes of 0.25, 1, 2, 10, and 20 nm have been used for various instruments. At each wavelength step, the GLAMR shutter is opened, illuminating the integrating sphere for a set duration known as the dwell time. Each dwell time is bracketed by a "dark period" with the GLAMR shutter closed, allowing the laser wavelength to be tuned to the next wavelength and the background signal collected. The lengths of the dwell times are dependent on the requirements for the DUT. For example, the dwell time for OLI-2 was 2 minutes but was only 40 seconds for the VIIRS instruments. The minimum dark period is dependent on the duration the GLAMR system requires to tune to the next wavelength. In preparation for the calibration, a full simulation of the test plan can be run to verify that all laser configurations are ready to support the scans. This simulation serves as a critical preparatory step, validating that all laser configurations are correctly set up to support the intended scans and establishing an additional layer of confidence in the testing protocol.

2.4. Data collection

GLAMR telemetry data including information such as wavelength reported by a wavemeter, signal from the three SMs and three TRs when in use, and shutter state are collected asynchronously between 1 and 5 Hz frequency. Real-time monitoring of radiance and wavelength status is enabled through visual displays and the data are recorded to the GLAMR data system in text files. Every telemetry point includes a timestamp recorded with microsecond precision. The stability of laser parameters such as wavelength, radiance and linewidth are monitored over time. When a measurement at an individual wavelength has been determined to be unstable based on instrument-specific stability requirements, the measurement is repeated. In post-processing, the data from the dark periods are averaged in order to perform background subtraction on the nearest-in-time illuminated data. The radiometer and wavemeter data are joined based on their timestamps.

In the data processing for the sphere calibration stage, the dark-corrected signals from the SMs (r_{SM}) and the TRs (r_{TR}) are used to calculate the unitless sphere calibration ratio r_{TR}/r_{SM}. Measurements of this ratio are made across the GLAMR wavelength range. During the instrument calibration stage, the absolute radiance of the integrating sphere is derived from the SM signals s_{SM} in digital number (DN) after its dark-signal correction and amplifier-gain adjustment. That is, for each GLAMR wavelength λ_k, the GLAMR sphere radiance $L(\lambda_k)$ reaching the DUT is calculated by

$$L(\lambda_k) = s_{SM} \cdot \frac{r_{TR}/r_{SM}}{g_{TR}}, \tag{1}$$

where the responsivity of the TR, g_{TR} in units of g_{TR} is DN/(W/m^{2}sr), is calibrated at NIST. Note that all variables are wavelength dependent, but the lambda subscript has been left off for simplicity.

The number of image frames acquired by the DUT during the dwell time varies by the instrument, depending on its detector characteristics including the integration time and SNR. The response of the DUT for each wavelength, denoted as $S(\lambda_k)$, are calculated by averaging the responses over all image frames. By pairing the GLAMR radiance from the sphere and the detector responses from the DUT at each λ_k, the ASR of the DUT detector and subsequently its RSR can be determined.

2.5. SI traceability

As mentioned above, the traceability of the GLAMR RadCal is established through a well-calibrated TR package. The entire calibration chain is visually represented in Fig. 3, showing the achievement of the SI-traceability for the GLAMR RadCal. The Primary Optical Watt Radiometer (POWR) is the United States′ primary standard for optical power measurements, and the source to which the radiometric calibration, including the detector-based calibration, is traceable. POWR is developed at NIST, with its optical power measurement traceable to SI units by the electrical substitution method, in which heating of a small cavity by optical absorption is matched to joule heating from an electrical resistance heater. Its measurement uncertainties are marked at 0.01% (k=1) [28]. With NIST′s own SIRCUS as the light source, a separate set of standard reference detectors are themselves calibrated directly against POWR first, and then used to calibrate the GLAMR TRs, again using SIRCUS tunable lasers as sources to establish the radiometric scales. Once calibrated, the GLAMR TRs are transported to the DUT test site, where they are used to calibrate the GLAMR SMs during a sphere calibration. These SMs are subsequently referenced to measure the GLAMR radiance during the DUT calibration.

3. Data processing and products

3.1. ASR derivation

The measurement of the detector spectral response functions, or instrumental profiles within the field of spectroscopy, is critical to assess the performance of the DUT. The primary product of the GLAMR RadCal is the ASR of instrument detectors. For each GLAMR wavelength, illuminated data are captured by the DUT during the dwell time and dark data are captured during the dark period. Each DUT image is checked for saturation. The means and standard deviations of the DUT images within a wavelength collection are calculated for the illuminated and dark periods, respectively and stored. The difference between the illuminated mean and the dark mean is the dark-corrected instrument response $S(\lambda_k)$ for the wavelength. The values of GLAMR wavelengths λ_k and radiance $L(\lambda_k)$ are retrieved from the GLAMR dataset by timing alignment. Therefore, for each instrument detector, its ASR for wavelength λ_k is calculated by

$$ASR_{\lambda_k} = \frac{S(\lambda_k)}{L(\lambda_k)}. \tag{2}$$

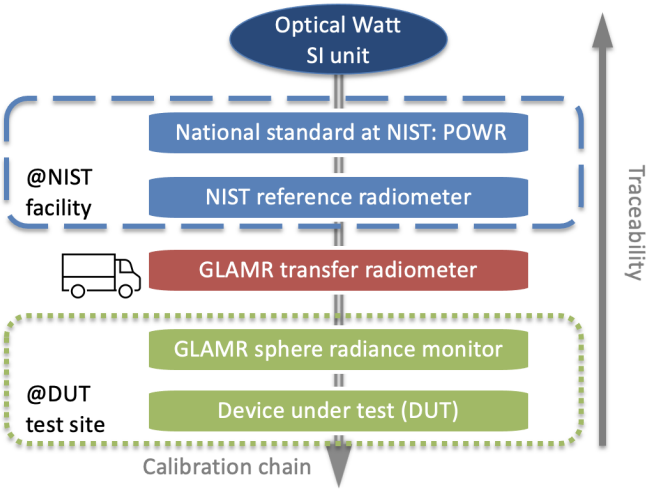

Fig. 3. A visual representation of the GLAMR RadCal calibration chain, and the completion of SI-Traceability.

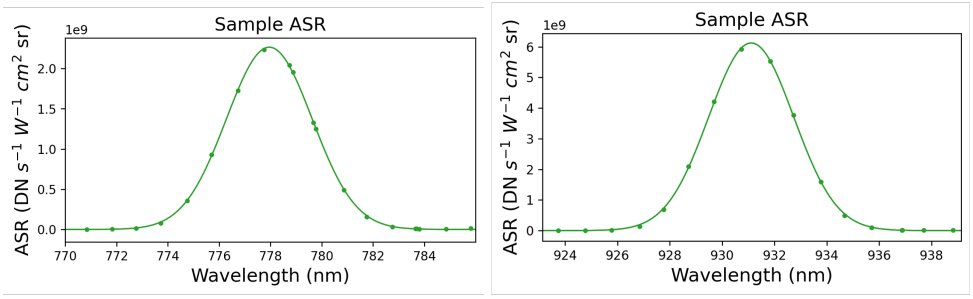

(a) (b)

Fig. 4. Sample ASRs. The dots denote measured values with the curves their Gaussian fitting.

The resulting ASRs are expressed in units of detector count per radiance, or DN/(W/m^{2}sr) in SI units. The calculation is repeated for all detectors of the DUT. As an example, Fig. 4 shows the ASRs measured for two sample detectors of an imaging spectrometer. The detectors chosen were for the same spatial location on the focal plane but from two different spectral locations with peak responses at 778 and 932 nm, respectively. The nominal bandwidths of the instrument at these two detectors are approximately 4.5 nm and the spectral sampling interval was 1 nm at its nominal value. The actual wavelength intervals spread within a range around the nominal value due to the limitation in perfectly controlling the output laser wavelength.

3.2. Band/detector parameters

The calibrated detector ASR carries comprehensive information about the detector responsivities. Furthermore, ASR can be used to derive various standard parameters typically referenced to characterize the performance of an instrument detector, or a spectral band, including the band-integrated responsivity R_{BI}, center wavelength (CW) λ_{BA}, and bandwidth (BW) or the Full Width at Half Maximum (FWHM), and RSR [29]. The actual ASR is a continuous function of wavelength, so these parameters are theoretically calculated through the integration

of corresponding physical characteristics. In practice, these integrals are numerically computed from discrete ASRs calibrated from GLAMR RadCal. The trapezoidal summation rule is adopted as the baseline integration method since it is less sensitive to irregular, and sometimes narrow wavelength intervals, which is frequently encountered during GLAMR laser scanning.

In real applications, the DUT detectors are mostly exposed to broadband light sources, such as sunlight reflected off Earth′s landscape or direct sunlight. Therefore, the efficiency of a detector/band in converting incoming radiance into the electric signals is usually represented by its band-integrated responsivity R_{BI} in units of DN·nm/s/(W/cm^{2}sr). Its value can be calculated by performing a trapezoidal summation of the detector ASR across the spectral region, as follows:

$$R_{BI} = \sum_{k=2}^{k_{max}} [\frac{ASR(\lambda_k) + ASR(\lambda_{k-1})}{2}][\lambda_k - \lambda_{k-1}], \tag{3}$$

where k_{max} is the number of GLAMR wavelengths scanned during calibration. The summation could be done using various other approaches like mid-point rule or Simpson′s rule, which essentially connects the ASR data points in different ways. Equation (3) assumes the input light is monochromatic or near monochromatic. A convolution between the ASR and the radiant spectrum need to be enacted for better accuracy.

Similarly, the band-averaged CW of a detector is calculated by

$$\lambda_{BA} = \frac{\sum_{k=2}^{k_{max}} \lambda_k ASR(\lambda_k) + \lambda_{k-1} ASR(\lambda_{k-1})}{\sum_{k=2}^{k_{max}} ASR(\lambda_k) + ASR(\lambda_{k-1})} \tag{4}$$

and the bandwidth is calculated by

$$BW = \frac{1}{\alpha} \sum_{k=2}^{k_{max}} [\frac{ASR(\lambda_k) + ASR(\lambda_{k-1})}{2}][\lambda_k - \lambda_{k-1}], \tag{5}$$

where α is the peak responsivity of the detector. Once again, the trapezoidal rule is used for the summation while other integration rules can be applied. The summations are carried out across both the in-band region and the out-of-band region. The FWHM is another commonly used measure of the spectral width of a detector, bracketed by the two wavelengths with 50% of the peak responsivity.

Another key metric of the detector performance, the RSR, is calculated by the normalization of the ASR as follows

$$RSR = \frac{ASR}{\alpha}. \tag{6}$$

The resulting dimensionless RSR describes how the detector response varies across the spectrum.

4. Uncertainty sources

With broadband light source, the detector′s response can be estimated by multiplying R_{BI} with the band-averaged spectral radiance received by the detectors. Hence, any inaccuracy in the calibrated R_{BI} is proportionally propagated to the uncertainty of the radiometric measurements, making it a crucial parameter for assessing the uncertainty in the GLAMR RadCal process. Combining Eqns (1) to (3), R_{BI} is calculated by its integral form as

$$R_{BI} = \int \frac{\overline{S(\lambda)}}{\overline{s_{SM}(\lambda)} \cdot \frac{r_{TR}/r_{SM}(\lambda)}{g_{TR}(\lambda)}} \, d\lambda. \tag{7}$$

In the equation, the averages of the DUT response $S(\lambda)$ and SM response $s_{SM}(\lambda)$ are over their corresponding data collection periods, respectively. The various sources of uncertainty for the

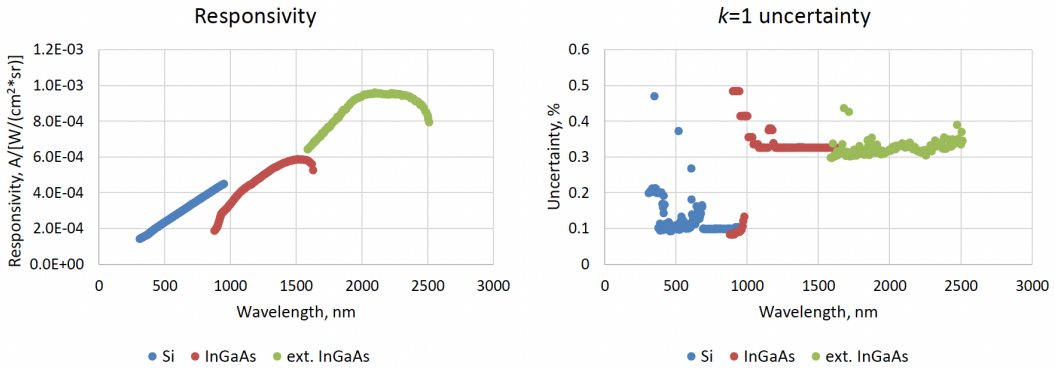

Fig. 5. The spectral responsivity of the TR and the associated uncertainty measured by NIST.

GLAMR RadCal can be identified and assessed through recent tests, including the RadCal of SOLARIS and OCI conducted in 2018 and 2022, respectively. This assessment is essential in ensuring the accuracy and reliability of the GLAMR RadCal measurements. For ease of analysis, these sources of uncertainty are categorized based on: those originating from the calibration standard (*i.e.*, the transfer radiometer), those inherent to the GLAMR system, and those based on the test configuration.

4.1. Calibration standard: transfer radiometer

The primary source of uncertainty in the GLAMR RadCal is linked to the uncertainty of the TRs, the calibration standard that carries the SI traceability for the RadCal. NIST directly provides the absolute spectral responsivities of these detectors along with the associated uncertainty of their calibration to the GLAMR team, a sample of which is shown in Fig. 5 [30]. This uncertainty is spectrally dependent and is primarily dictated by choice of the transfer standard detectors used by NIST SIRCUS to transfer the radiometric scale from the SIRCUS cryogenic radiometer to the GLAMR TRs. The typical values of uncertainty for these three types of detectors are 0.15%, 0.35% and 0.35%, respectively. Maintaining the accuracy and reliability of the TR traceability is vital to ensuring the overall traceability of the GLAMR RadCal. While the semiconductors themselves are expected to be stable, instabilities could arise from changes in auxiliary optical and electronics components. To minimize the associated uncertainty, the TRs and their accompanying amplifiers are regularly re-calibrated by NIST after each GLAMR RadCal.

4.2. GLAMR system

To build upon the overall uncertainty budget for the GLAMR RadCal, the uncertainties induced from various components of the GLAMR system are assessed individually below.

4.2.1. Light source

For each GLAMR tuned wavelength during the GLAMR RadCal, the radiance within the sphere is measured using the SM and the wavelength on the laser table is measured using a wavemeter. Both the radiance and wavelength can fluctuate within the dwell time. Typical variabilities of the GLAMR radiance and wavelength, quantified as the root-mean-square error (RMSE) of the SM and wavemeter readings, can be estimated from past GLAMR RadCal. It is noted that the noise of the SM and wavemeter is incorporated into these variabilities. An illustrative example of this assessment is shown in Fig. 6 with data from the recently executed HySICS GLAMR RadCal. Additional data from prior GLAMR RadCal also suggest that radiance variation generally peaks

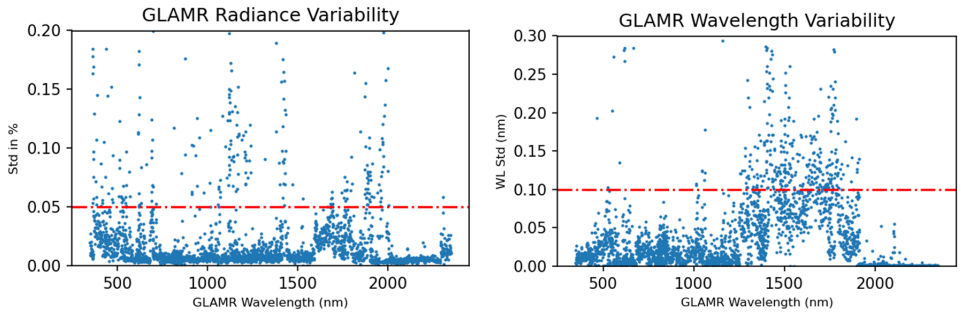

(a) (b)

Fig. 6. The variability of GLAMR (a) radiance and (b) wavelength within the dwell time of a GLAMR wavelength. The data are collected from the GLAMR RadCal of HySICS, which was conducted in September, 2023. The red dashed lines denote the UC budgets for the variability. The wavelength collections beyond have been re-measured at the end of the RadCal.

at 0.05%, while wavelength variation remains below 0.1 nm. The fluctuations in radiance and wavelength introduce uncertainty to the detector output within the dwell time, in addition to the inherent detector noise. Those wavelength collections with significantly larger variations in radiance or wavelength are subject to re-scanning in go-back measurements and thus can be excluded from uncertainty budgeting consideration. Therefore, the laser variability in the data actually used in calibrating ASRs could be less than the peaks depicted in Fig. 6.

The variation in detector output is directly proportional to radiance variation, peaking likewise at 0.05%. However, it is the averages of the measured radiance and wavelength with a dwell time that are used as inputs for the ASR calculation according to Eqn. 2. Given that the variation is largely a random process and many samples of the GLAMR data are gathered within a dwell, the standard error of the measurements is considerably reduced. Consequently, the contribution of the radiance variation to the calibration uncertainty is budgeted at 0.02%. The effect of the wavelength variation is more subtle, and will be explained in section 4.3.2. Given that the variability in laser radiance and wavelength is a stochastic process, their contribution to the overall uncertainty can usually be mitigated by extending the dwell time and increasing the number of captured data points. However, as increasing the number of wavelength steps extends the total testing time, this requirement can occasionally pose a scheduling challenge for the GLAMR RadCal.

In a laser system like GLAMR, unintended transmission of different wavelengths from various elements of the system could occur. This can lead to spurious results in the instrument calibration. In particular, fundamental wavelength transmission through the second harmonic generator remains co-aligned with the second harmonic output and can be coupled to the fiber if not adequately filtered. The amount of fundamental light transmitted can be quantified by a dedicated spectral measurement of the sphere with a spectroradiometer at selected laser illumination wavelengths. One example is shown in Fig. 7, where fundamental light was observed mixed with the second harmonic output during a pre-test sphere calibration for HySICS. This was corrected by adding dichroic filters to the second harmonic OPO and was verified by repeating the measurement. Spectral measurements are crucial to identify and quantify any unexpected spectral components in the output radiance. By regularly incorporating this measurement into the testing process to verify the lack of fundamental wavelength leakage, the contribution of additional spectral content to the overall uncertainty can effectively be budgeted at zero. This method ensures that any undesired spectral crosstalk is identified and corrected, enhancing the

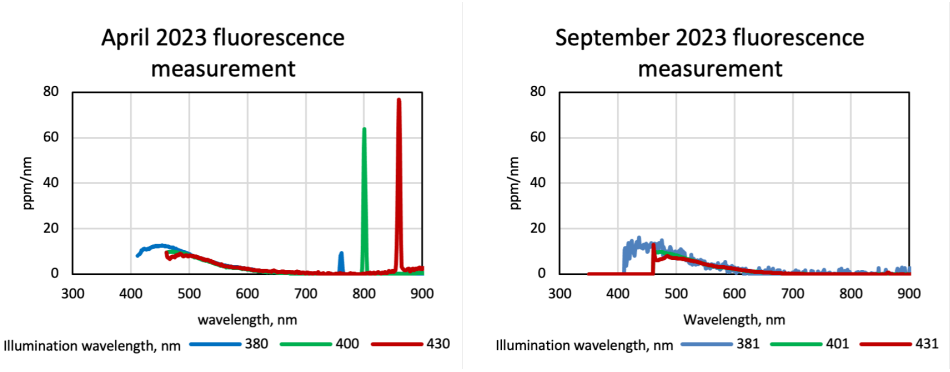

(a) (b)

Fig. 7. Spectral contents of GLAMR output radiance before (April, 2023, a) and after (September, 2023, b) installation of additional dichroic filters..

accuracy of GLAMR RadCal and maintaining the system's integrity. In the example shown in Fig. 7, a broadband spectral component also appears. This is due to fluorescence of the integrating sphere itself (see section 4.2.3) and is not affected by the addition of the dichroic optics.

4.2.2. Sphere monitor non-linearity

Currently, the GLAMR calibration assumes a linear relationship in the SM/TR detector response ratio r_{SM}/r_{TR} and the amount of radiance exposed. Any deviation from the linearity in the detector response introduces uncertainty to the calibration. The non-linearity of theTR has been checked at the NIST beam conjoiner facility, and no detectable non-linearity has been found at photocurrents ranging from 10^{-8} to 10^{-5}A [31]. The non-linearity of the SM/TR detector response ratio, which is essentially the non-linearity of the SM detector response, has been examined at NASA using the sphere calibration configuration. Slight wavelength-dependent nonlinearity has been observed, as is shown in Fig. 8. Based on these tests, the uncertainty attributable to non-linearity is established at 0.02% for the associated spectral region. This uncertainty cannot be reduced by simply repeating measurements since the detector non-linearity is not a random process.

4.2.3. Integrating sphere

The internal coating of the GLAMR integrating sphere, while designed to be a perfect Lambertian diffuser, does not achieve total uniformity. As a result, variations in light reflection and deflection occur at different viewing positions or angles, contributing to measurement uncertainty [32]. This non-uniformity of the GLAMR sphere has been characterized at NASA using a scanning radiometer with a narrow field of view. The radiometer is positioned on an X-Y-θ alignment stage to scan the 20-cm sphere port in two orthogonal directions in 2-cm increments. In addition, the alignment stage allows an angular scanning of ±25° from the centerline in 1° increments [33]. The measurements are repeated at multiple GLAMR wavelengths. The results show spatial variability of ±0.1% horizontally and ±0.3% vertically, along with an angular non-uniformity of less than 0.1% within ±10°. The variation in uniformity does not show any significant dependence on the wavelength. An example of uniformity data is shown in Fig. 9.

During the GLAMR RadCal, the TR and the DUT are carefully staged at the same position, pointing to the centerline of the sphere port using an alignment guide such as a standard theodolite. Even if the alignment itself is perfect, the fields-of-views of the TRs and instrument detectors

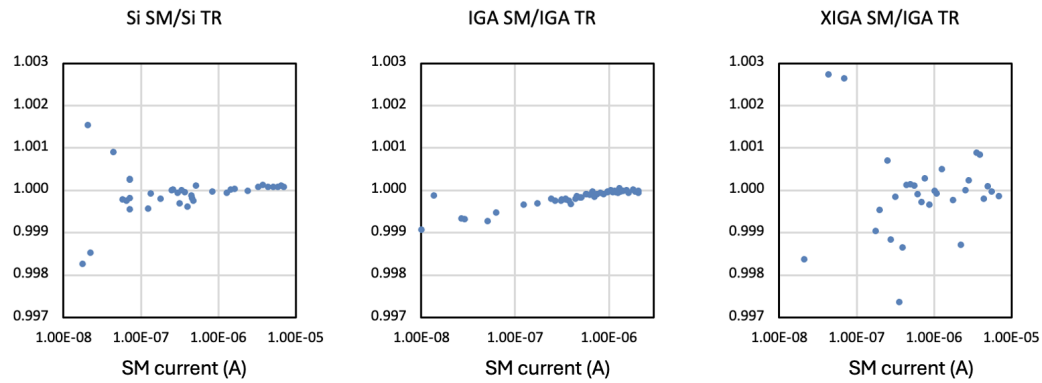

Fig. 8. The normalized SM/TR ratios from the non-linearity measurement. The GLAMR laser wavelengths for the measurement are 759 nm for silicon detector and 998 nm for IGA and XIGA detectors, respectively.

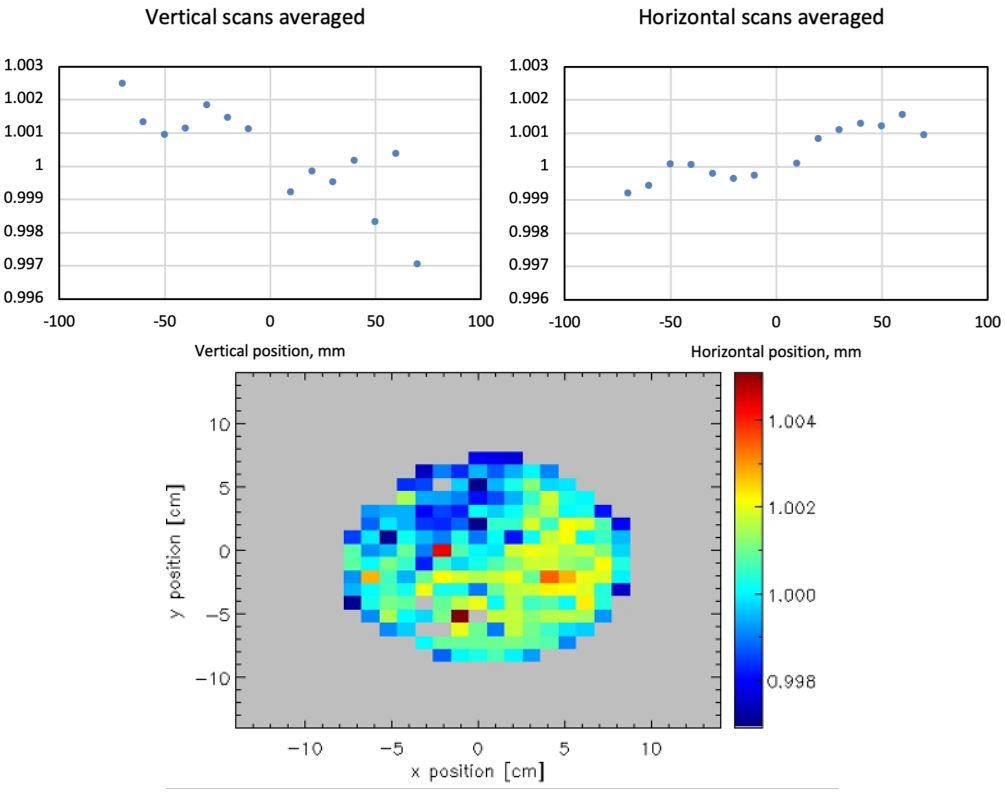

Fig. 9. The Integrating sphere uniformity assessment results at 850 nm. All values are ratios of the radiometer output relative to the center position at (0,0).

do not completely match. This mismatch, combined with the intrinsic sphere non-uniformity characterized above, causes potential measurement uncertainty. The uncertainty attributed to sphere non-uniformity is budgeted at 0.1%, an estimate representing the maximum value observed. This number aligns closely with an Independent sphere uniformity assessment performed by

NIST [34].

When laser light illuminates a diffuse object, it produces a random interference effect known as a speckle pattern that affects the uniformity of the output. The size and intensity of the speckle pattern depend on the surface roughness of the sphere's interior and the coherence properties of the laser light. laser speck is a highly localized effect. While the current sphere non-uniformity assessment may not be sufficiently precise in the spatial domain to gauge the impact of the speckle effect, the impact of laser speckle can be minimized by either hardware approach by adding a fiber de-speckler into the beam path, or software approach by smoothing signals from adjacent pixels. The choice of de-speckle method depends upon the instrument under calibration. Instruments with large field-of-view and wide bandwidth are generally insensitive to the speckle effect. Therefore, the uncertainty of laser speckle is not separately budgeted.

The coating of the integrating sphere emits low levels of UV and blue fluorescence when exposed to irradiation, causing extra uncertainty in calibrating this spectral region. This fluorescence, characterized by light emitted at a longer wavelength than the incident light and with a broader linewidth than the source of excitation, can introduce additional uncertainty in the calibration of spectral regions. The amount of fluorescence can be measured from the spectral measurement described above using a spectroradiometer. While the actual uncertainty induced by fluorescence depends on the instrument detector′s spectral response, past measurements such as the example shown in Fig. 7 indicate that the uncertainty from fluorescent emission to the overall uncertainty can be budgeted to be less than 0.05% at wavelengths shorter than 400 nm.

4.2.4. System repeatability

A complete GLAMR RadCal involves a multitude of measurements performed over a period of two weeks or longer, including the sphere calibration with the TR and the test with DUT. This sequence necessitates a high level of repeatability, meaning the outputs from the GLAMR system in these measurements under unchanged conditions should remain consistent. Uncertainty sources for the repeatability can stem from multiple devices within the GLAMR system, including those previously discussed. Variability in the GLAMR-based calibration due to these devices is expected to be minimal, but practical challenges in quantitatively assessing the variability of each one separately has not been done as of the writing of this paper. Instead, the system′s overall repeatability is evaluated by repeating the sphere calibration using the same setup at different times. The repeatability is estimated as the variability among these measurements as is shown in Fig. 10 over a time span of 3-6 months. Typically, the sphere calibration that determines the SM/TR detector response ratio, r_{SM}/r_{TR}, is scheduled separately from the actual DUT calibration within a month, resulting in reduced variability in the system between the calibrations.

In the water vapor absorption regions of 1350-1500 nm and 1800-2100 nm, it is notable that the repeatability of the sphere calibration is considerably degraded compared to other regions. The sphere and the related optical path are not purged and contain ambient air. The variability of water vapor content between measurements as well as the lower source radiance due to water vapor absorption lead to larger uncertainties. Prior to further verification, the uncertainty budget for the system repeatability is simply determined based on the variability observed in this measurement.

4.3. Test configuration

In addition to the intrinsic specifications of the GLAMR hardware, the operational setup and configuration of a GLAMR RadCal that includes aspects like the hardware setup, the laser wavelength scanning strategy, the determination of the test schedule, as well as the selection of data and its processing algorithm can all introduce uncertainties to the overall budget. While the objective of the test planning is to minimize these contributions, they can often still be significant due to constraints in the testing.

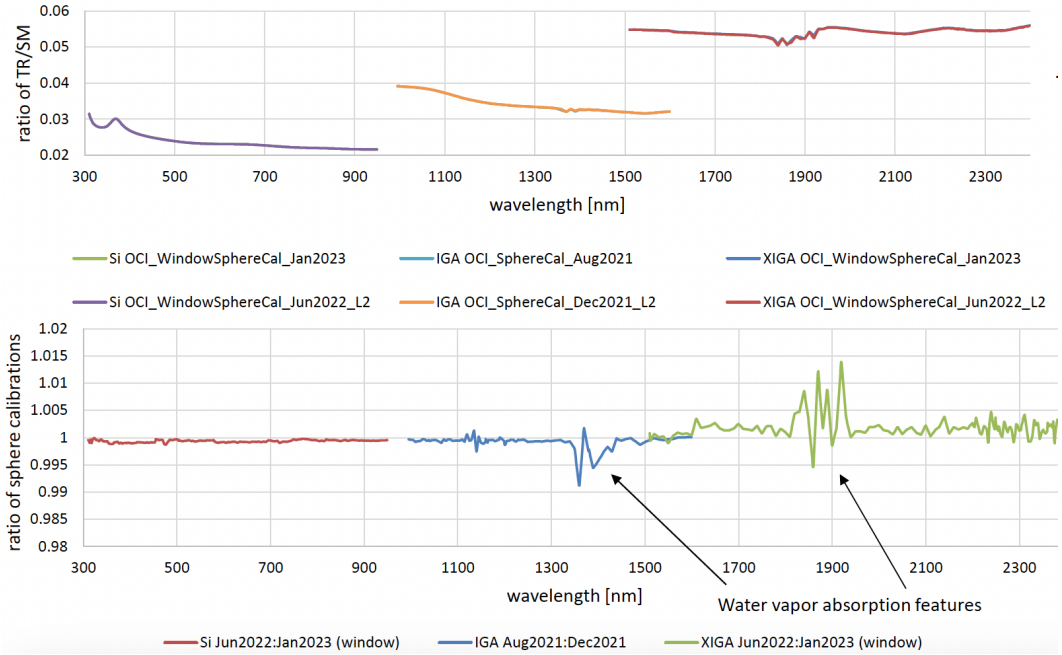

Fig. 10. The comparison of repeated sphere calibrations under the same configuration to demonstrate the system repeatability of the GLAMR RadCal. In the top chart, each segment of the curve comprises two overlapping lines from the same radiometer measured at two different times. Their ratios are presented in the bottom chart.

4.3.1. Spectral sampling

The spectral tuning of lasers in the GLAMR system is through the adjustment of the LBO temperature and the prism stages. This process is fully automated, which facilitates significantly faster data collection rates compared to manual optics adjustment. Typically, tuning between wavelengths at 1 nm increments requires between 30 to 60 seconds, though larger increments might necessitate more time. When operating for 16 hours a day in double-shift mode, the GLAMR team can scan 300 to 400 wavelengths daily. This means the full spectral range of the OPO is scanned in about 4 to 5 days with 1-nm intervals.

For a multispectral instrument featuring typical bandwidths of 20 nm or more, a 1-nm sampling step is sufficiently small enough to limit the uncertainties in determining the band-integrated and band-averaged response values. However, to calibrate instruments with much narrower spectral bandpasses of only a few nanometers, the uncertainty can increase noticeably due to the under-sampling of the ASR in the spectral domain. A Monte-Carlo simulation of the GLAMR RadCal, which is conducted based on the modeled ASR values of the DUT to predict the detectors' outputs under various testing parameters [35], reveals that the uncertainty due the discrete sampling, in terms of the RMSE of the band-integrated responsivity R_{BI}, ranges from 0.15% to 0.20% when the ASR is measured at 1-nm sampling interval. It is anticipated that this uncertainty would decrease to 0.05% when the sampling interval is reduced to 0.5 nm or less. Figure 11 demonstrates the relationship between the uncertainty introduced by this spectral under-sampling effect at various laser wavelength intervals. Accordingly, a constant uncertainty budget of 0.05% is assigned to the spectral sampling effect, regardless of the specific instrument. However, this could present challenges in test setup, as it would require doubling the duration and effort of testing compared to a 1-nm interval.

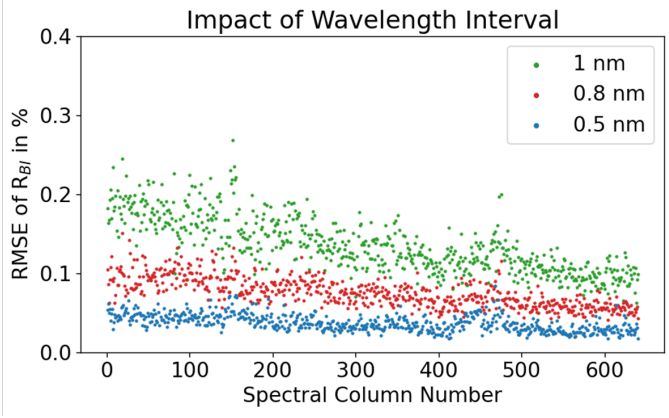

Fig. 11. The uncertainty due to the spectral under-sampling at varioius GLAMR sampling intervals/wavelength steps. The values are calculated from a simulation of the HySICS GLAMR RadCal. The bandwidths of the HySICS detectors increase with the spectral column numbers, resulting smaller uncertainties at fixed sampling interval.

4.3.2. Laser wavelength variability

Unlike the case for laser radiance variation, the effect of the wavelength variation is largely contingent on the spectral responses of the DUT, or particularly the bandwidth. For instance, the response of a spectrometer detector with a bandwidth of just a few nanometers is more sensitive to laser wavelength variation than a multispectral sensor detector with a bandwidth of several dozen nanometers. This increased sensitivity is due to the steeper slope of a larger portion of the in-band ASR. The uncertainty of the laser wavelength variability can only be estimated for each instrument taking into account its design parameters, and is thus categorized as a component of test configuration. Based on several multi-spectral instruments calibrated by GLAMR, its impact to the calibration uncertainty is conservatively budgeted at 0.04%. The value for a spectrometer could be much greater.

4.3.3. TR/Instrument alignment

Establishing the traceability of GLAMR RadCal requires the co-alignment of the TR during sphere calibration and the DUT during the test. This process uses a theodolite to align the instrument's boresight to the centerline of the port of the integrating sphere. A significantly larger mis-alignment error can further increase the spatial non-uniformity of the output radiance from the sphere which has been budgeted at 0.1%. No measurement has been carried out to directly quantify the relationship between the degree of mis-alignment and the resulting uncertainty. Since existing GLAMR RadCal results do not suggest any significant increase in uncertainty due to alignment issues alone, its contribution to the overall uncertainty is not separately budgeted.

4.3.4. Data processing algorithm

The strategies for data selection and the processing algorithms can significantly impact the calibration results in many ways. For example, several approaches can be used to conduct the numerical integration to compute the R_{BI} from the ASR by Eqn. 3, two of which include Trapezoidal summation and Simpson′s rules. The simulation results described in 4.3.1 suggest a discrepancy of up to 0.02% in the integrated values, based on 25 valid data samples taken within the in-band ASR. Since the exact shape of the detector ASR is not known, it is difficult to determine which approach is superior. As such, this uncertainty is budgeted accordingly.

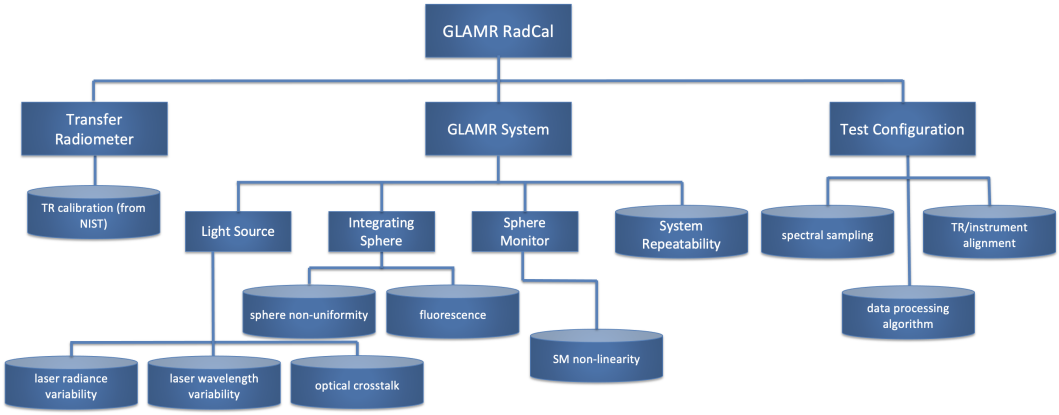

Fig. 12. The breakdown of the uncertainty sources of GLAMR RadCal. The terms in the cylinders are individual uncertainty sources included in the overall RSS budget.

Furthermore, the laser tuning process often results in a larger spectral gap than the set wavelength interval, leading to increased uncertainty in the numerical integration process. When defining the test, it is crucial to allow for "go-back" measurements, which involve tuning the laser to the center of the gap to fill it during subsequent measurements, helping to mitigate this source of uncertainty.

5. Uncertainty budget and analysis

With the measurement process defined and uncertainty sources identified, the uncertainty budget of the GLAMR RadCal is created. The associated uncertainty diagram is shown in Fig. 12, partitioning the total uncertainty inherent in the GLAMR RadCal into its components. This diagram offers a detailed visualization of how each part quantified in Section 4 contributes to the aggregate uncertainty. The contribution from each uncertainty source is summarized for the spectral range from 350 nm to 2300 nm in Table 3. All uncertainty values correspond to a coverage factor of k=1. The overall root sum square (RSS) combined GLAMR RadCal uncertainty budget is presented in Table 4. The terms found in the cylinders in Fig. 12 represent the individual uncertainty sources included in the overall RSS calculation.

Table 3. A breakdown of the reflective solar band calibration uncertainty (k=1) for each component for GLAMR RadCal

		UV	VIS	NIR	NIR	SWIR	SWIR	SWIR
Wavelength (nm)		350-400	400-950	950-1350	1350-1500*	1500-1800	1800-2100*	2100-2300
Transfer Radiometer	TR calibration (from NIST)	0.20%	0.15%	0.35%	0.35%	0.35%	0.35%	0.35%
GLAMR System	laser radiance variability	0.02%	0.02%	0.02%	0.02%	0.02%	0.02%	0.02%
	TR/SM non-linearity	0.02%	0.02%	0.02%	0.02%	0.02%	0.02%	0.02%
	sphere non-uniformity	0.10%	0.10%	0.10%	0.10%	0.10%	0.10%	0.10%
	sphere fluorescence	0.05%	0%	0%	0%	0%	0%	0%
	system repeatability	0.04%	0.04%	0.04%	0.80%	0.25%	1.20%	0.40%
Test Configuration (Instrument Dependent)	spectral sampling	0.05%	0.05%	0.05%	0.05%	0.05%	0.05%	0.05%
	laser wavelength variability	0.04%	0.04%	0.04%	0.04%	0.04%	0.04%	0.04%
	data processing algorithm	0.02%	0.02%	0.02%	0.02%	0.02%	0.02%	0.02%

*: water vapor absorption regions

Table 4. Overall GLAMR RadCal uncertainty budget (k=1)

	UV	VIS	NIR	NIR	SWIR	SWIR	SWIR
Wavelength (nm)	350-400	400-950	950-1350	1350-1500	1500-1800	1800-2100	2100-2300
RSS Combined	0.24%	0.20%	0.38%	0.88%	0.45%	1.26%	0.55%

The uncertainty budget offers an overview of the potential sources of uncertainty within the GLAMR RadCal process. It serves as a tool for improving the precision and accuracy of the measurements. It should be noted that the budgeting is conducted based on our current knowledge of the GLAMR system and the RadCal setup. It presumes certain conditions are satisfied, such as the absence of significant stray light sources. The values in Tables 3 and 4 provide the baseline of GLAMR RadCal UC that demonstrates the optical performance of the GLAMR system. As is noted in the table, some numbers are contingent to the DUT and test configurations, and are subject to increase. Given the spectral responses of DUT detectors, the uncertainty of its GLAMR RadCal will need to be re-assessed more accurately on a case-by-case basis.

GLAMR RadCal has yet to reach the accuracy requirements sufficient to observe climate change to within the uncertainty of the limit of natural variability, which stands at 0.3% (k=2) for the reflected solar spectrum. The TR traceability was originally studied for an irradiance source for the SIRCUS RadCal at NIST [16]. The TR uncertainty is at a much lower value of 0.09% (k=3). The significant elevation in uncertainty levels in GLAMR RadCal can be mostly attributed to the choice to calibrate radiance using a sphere source instead of irradiance, with the advantage that a radiance source used in the calibration of the sensor can reflect real-world operational conditions more accurately. Simultaneously, the GLAMR team at NASA has been continuously working on improving the GLAMR system and fine-tuning the calibration configuration to minimize their contribution to the GLAMR RadCal. For example, the spectral measurement proposed previously to address fluorescence and spectral leak has been adopted as a routine procedure. Purging the sphere of water vapor would significantly reduce the uncertainties in the water vapor absorption spectral regions. Efforts also are underway to develop methods to assess and verify this uncertainty budget through assessment of the results of previous GLAMR RadCal for several instruments such as Landsat-9 OLI-2 and Goddard Institute for Space Studies (GISS) Research Scanning Polarimeter (RSP). Both GLAMR RadCal and sphere-based absolute RadCal have been conducted for these instruments, so the detector responsivities calculated from the GLAMR-based calibration and those from traditional source-based methods can be cross-checked. While the traditional RadCal approach is expected to have larger uncertainty than GLAMR RadCal, such comparisons are expected to indicate if there is a major issue in GLAMR RadCal error budget shown here. Consistent results between the two sets of results would confirm no major uncertainty sources were overlooked in our budgeting process.

6. Conclusion

One realization of the detector-based, absolute radiometric calibration approach has been successfully achieved at NASA GSFC with the GLAMR system. This radiance-based calibration approach relies on a tunable laser system to illuminate an integrating sphere as a light source, and a reference TR separately calibrated at NIST to determine the output radiance from the sphere for the calibration of the DUT. Through tuning the laser source across the entire spectral range of the DUT, the ASR of the detectors is measured, providing the necessary data for both in band and out-of-band characterization of the detector performance.

This paper thoroughly investigates the uncertainties associated with the GLAMR RadCal. It explores potential sources of uncertainty tied to the GLAMR system itself, the configuration of the test, and the methods employed for data processing. A detailed analysis is conducted to

gauge the impact of each source of uncertainty, identifying the most significant contributors. In conclusion, the calibration uncertainty of GLAMR RadCal is assessed to be better than 0.3% (k=1) within the 350-950 nm wavelength range and 0.6% (k=1) within the 950-2300 nm range, excluding water-vapor absorption regions. This represents a notable improvement compared to conventional RadCal approaches. This suggests the GLAMR RadCal holds significant potential for enhancing the RadCal quality of the future remote sensing instruments operated within the reflective solar ranges. Moreover, this study presents practical recommendations on how to refine the calibration process to lower these uncertainties.

Funding. This research was funded by the CLARREO Pathfinder Project, with additional support from other projects associated to GLAMR calibration, that includes the JPSS, the PACE and the Landsat programs.

Acknowledgments. The authors would like to extend their gratitude towards the NASA/GSFC GLAMR team for their immense dedication and efforts in the development and operation of the system.

Disclosures. The authors declare no conflicts of interest.

Data availability. Data underlying the results presented in this paper are not publicly available at this time but may be obtained from the authors upon reasonable request.

Supplemental document. No supporting content is attached to this publication.

References

1. K. Thome and Y. Aytac, "Independent calibration approach for the clarreo pathfinder mission," in *Proc. SPIE,* vol. 11130 (2019), p. 111300B.
2. B. A. Wielicki, D. F. Young, M. G. Mlynczak, K. J. Thome, S. Leroy, and J. Corliss, "Achieving climate change absolute accuracy in orbit," Bull. Am. Meteorol. Soc. **94**, 1519–1539 (2013).
3. "Clarreo pathfinder mission," Available Online: https://clarreo-pathfinder.larc.nasa.gov/ (accessed on 20 Dec 2023).
4. G. Kopp, P. Smith, C. Belting, Z. Castleman, G. Drake, J. Espejo, K. Heuerman, J. Lanzi, and D. Stuchlik, "Radiometric flight results from the hyperspectral imager for climate science (hysics)," Geosci. Instrum. Method. Data Syst. **6**, 169–191 (2017).
5. X. Xiong, J. Sun, A. Wu, K.-F. Chiang, J. Esposito, and W. Barnes, "Terra and aqua modis calibration algorithms and uncertainty analysis," in *Proc. SPIE,* vol. 5978 (2005), p. 59780V.
6. X. Xiong, A. Angal, W. L. Barnes, H. Chen, V. Chiang, X. Geng, Y. Li, K. Twedt, Z. Wang, and et al., "Updates of moderate resolution imaging spectroradiometer on-orbit calibration uncertainty assessments," J. Appl. Remote. Sens. **12**, 034001 (2018).
7. C. Cao, J. Xiong, S. Blonski, Q. Liu, S. Uprety, X. Shao, Y. Bai, and F. Weng, "Suomi NPP VIIRS sensor data record verification, validation, and long-term performance monitoring," J. Geophys. Res. Atmosphere **118**, 11664–11678 (2013).
8. C. Cao, F. J. D. Luccia, X. Xiong, R. Wolfe, and F. Weng, "Early on-orbit performance of the visible infrared imaging radiometer suite onboard the suomi national polar-orbiting partnership (s-npp) satellite," IEEE Trans. Geosci. Remote. Sens. **52**, 1142–1156 (2014).
9. X. Xiong, J. Butler, K. Chiang, B. Efremova, J. Fulbright, N. Lei, J. McIntire, H. Oudrari, J. Sun, Z. Wang, and A. Wu, "VIIRS on-orbit calibration methodology and performance," J. Geophys. Res. Atmosphere **119**, 5605–5078 (2013).
10. D. Moyer, A. Angal, H. Oudrari, E. Haas, Q. Ji, F. D. Luccia, and X. Xiong, "Jpss-1 viirs prelaunch reflective solar band testing and performance," Remote. Sens. **14**, 5113 (2022).
11. D. Moyer, A. Angal, Q. Ji, J. McIntire, and X. Xiong, "Jpss-2 viirs prelaunch reflective solar band testing and performance," Remote. Sens. **14**, 6353 (2022).
12. B. Markham, J. Barsi, G. Kvaran, L. Ong, E. Kaita, S. Biggar, J. Czapla-Myers, N. Mishra, and D. Helder, "Landsat-8 operational land imager radiometric calibration and stability," Remote. Sens. **6**, 12275–12308 (2014).
13. B. L. Markham, D. Jenstrom, J. G. Masek, P. Dabney, J. A. Pedelty, J. A. Barsi, and M. Montanaro, "Landsat 9: status and plans," in *Proc. SPIE,* vol. 9972 (2016), p. 99720G.
14. J. Nieke and C. Mavrocordatos, "Sentinel-3a: commissioning phase results of its optical payload," in *Proc. SPIE,* vol. 10562 (2017), p. 105620C.
15. A. Deru, L. Bourg, N. Lamquin, S. Hunt, and S. Dransfeld, "Olci L1 radiometric uncertainties validation," in *CALCON,* (2022). https://digitalcommons.usu.edu/calcon/CALCON2022/All2022Content/23/.
16. S. W. Brown, G. P. Eppeldauer, and K. R. Lykke, "Facility for spectral irradiance and radiance responsivity calibrations using uniform sources," Appl. Opt. **45**, 8218–8237 (2006).
17. J. T. Woodward, P.-S. Shaw, H. W. Yoon, Y. Zong, S. W. Brown, and K. R. Lykke, "Invited article: Advances in tunable laser-based radiometric calibration applications at the national institute of standards and technology, usa," Rev. Sci. Instruments **89**, 091301 (2016).

18. J. McIntire, D. Moyer, S. W. Brown, K. R. Lykke, E. Waluschka, H. Oudrari, and X. Xiong, "Monochromatic measurements of the jpss-1 viirs polarization sensitivity," Appl. Opt. **55**, 7444–7454 (2016).
19. B. McAndrew, J. McCorkel, T. Shuman, B. Zukowski, A. Traore, M. Rodriguez, S. Brown, and J. Woodward, "Goddard laser for absolute measurement of radiance for instrument calibration in the ultraviolet to short wave infrared," in *2018 Conference on Lasers and Electro-Optics (CLEO),* (2018), pp. 1–2.
20. J. A. Barsi, J. McCorkel, B. McAndrew, B. Zukowski, T. Shuman, S. Johnston, and B. Markham, "Spectral testing of the Landsat-9 OLI-2 instrument using the Goddard Laser Absolute Measurement of Radiance (GLAMR)," in *Proc. SPIE,* vol. 10764 (2018), p. 1076405.
21. Z. Wang, K. Thome, R. Lockwood, and B. N. Wenny, "Absolute radiometric calibration of an imaging spectroradiometer using a laboratory detector-based approach," Remote. Sens. **14**, 2245 (2022).
22. "International vocabulary of metrology – basic and general concepts and associated terms (VIM)," (2006). Available Online: https://www.nist.gov/system/files/documents/pml/div688/grp40/International-Vocabulary-of-Metrology.pdf (accessed on 20 Dec 2022).
23. C. Wyatt, *Radiometric calibration: theory and methods* (Elsevier, 1978), 1st ed.
24. K. Thome, B. Markham, J. Barker, P. Slater, and S. Biggar, "Radiometric calibration of landsat," Opt. Sci. **63**, 853–858 (1997).
25. S. Brown, G. Eppeldauer, and K. Lykke, "NIST facility for spectral irradiance and radiance responsivity calibrations with uniform sources," Metrologia **37**, 579 (2000).
26. B. McAndrew and J. McCorkel, "Time resolved irradiance of an integrating sphere illuminated by a mode-locked optical parametric oscillator," in *Proc. SPIE,* vol. 11127 (2019), p. 111270K.
27. B. McAndrew, "Goddard laser for absolute measurement of radiance," in *Surface Biology and Geology Community Workshop,* (2019).
28. J. M. Houston and J. P. Rice, "NIST reference cryogenic radiometer designed for versatile performance," Metrologia **43**, S31–S35 (2006).
29. R. A. Barnes, S. W. Brown, K. R. Lykke, B. Guenther, J. J. Butler, T. Schwarting, K. Turpie, D. Moyer, F. DeLuccia, and C. Moeller, "Comparison of two methodologies for calibrating satellite instruments in the visible and near-infraed," Appl. Opt. **54**, 10376–10396 (2015).
30. "Report of test absolute spectral radiance responsivity of the NASA GLAMR Si radiometer model LTD-11, S/N 104," Available Online: https://glamr.gsfc.nasa.gov/uncertainty (accessed on 20 Dec 2023).
31. H. W. Yoon, "NIST test report id 685/srs2019-004 through -006," Available Online: https://glamr.gsfc.nasa.gov/uncertainty (accessed on 20 Dec 2023).
32. L. Hanssen, "Integrating-sphere system and method for absolute measurement of transmittance, reflectance, and absorptance of specular samples," Appl. Opt. **40**, 3196–3204 (2001).
33. B. McAndrew, J. Barsi, A. Sushkov, and J. McCorkel, "Radiometric uncertainty analysis of the glamr calibration facility," in *CALCON,* (2023). https://ntrs.nasa.gov/citations/20230007374.
34. K. Thome, J. McCorkel, and B. McAndrew, "Demonstrating the error budget for the climate absolute radiance and refractivity observatory through solar irradiance measurements," in *Proc. SPIE,* vol. 9607 (2015), p. 96071C.
35. Z. Wang, K. Thome, R. Lockwood, and B. Wenny, "A detector-based absolute radiometric calibration simulation for a climate-quality imaging spectrometer," in *Proc. SPIE,* vol. 12235 (2022), p. 122350H.